10.1590/s1982-21702018000300021

ARTICLE

A LIGHTWEIGHT UAV-BASED LASER SCANNING SYSTEM FOR FOREST APPLICATION

Um sistema de varredura a laser leve baseado em VANT para aplicação florestal

Fernanda Magri Torres[1] - ORCID: 0000-0002-9284-9145

Antonio Maria Garcia Tommaselli[1] - ORCID: 0000-0003-0483-1103

[1]Universidade Estadual Paulista (Unesp), Departamento de Cartografia,
Presidente Prudente - São Paulo, Brasil.
E-mail: fernanda.mt91@gmail.com; a.tommaselli@unesp.br

Received in October 2nd, 2017

Accepted in May 6th, 2018

Abstract:

Lightweight Unmanned Aerial Vehicles (UAVs) have become a cost effective alternative for studies which use aerial Remote Sensing with high temporal frequency requirements for small areas. Laser scanner devices are widely used for rapid tridimensional data acquisition, mainly as a complementary data source to photogrammetric surveying. Recent studies using laser scanner systems onboard UAVs for forestry inventory and mapping applications have presented encouraging results. This work describes the development and accuracy assessment of a low cost mapping platform composed by an Ibeo Lux scanner, a GNSS (Global Navigation Satellite System) antenna, an Inertial Navigation System Novatel Span-IGM-S1, integrating a GNSS receiver and an IMU (Inertial Measurement Unit), a Raspberry PI portable computer and an octopter UAV. The system was assessed in aerial mode using an UAV octopter developed by SensorMap Company. The resulting point density in a plot with trees concentration was also evaluated. The point density of this device is lower than conventional Airborne Laser Systems but the results showed that altimetric accuracy with this system is around 30 cm, which is acceptable for forest applications. The main advantages of this system are their low weight and low cost, which make it attractive for several applications.

Keywords: Mobile LASER Scanning System; UAV; mapping tool; point cloud.

How to cite this article: Torres, F.M. and Tommaselli, A.M.G. A lightweight uav-based laser scanning system for forest application. *Bulletin of Geodetic Sciences*, Vol. 24 (3): 318-334, Jul-Sept, 2018.

Resumo:

Veículos aéreos não tripulados (VANT) leves tornaram-se uma alternativa de baixo custo para estudos que dependem de Sensoriamento Remoto aéreo com alta frequência temporal em pequenas áreas. Dispositivos de varredura a LASER são amplamente utilizados para aquisição rápida de dados tridimensionais, principalmente como uma fonte de dados complementar ao levantamento fotogramétrico. Estudos recentes utilizando sistemas de varredura a LASER embarcados em VANT para aplicações de inventário florestal e mapeamento apresentaram resultados positivos. Este trabalho descreve o desenvolvimento e avaliação de uma plataforma de mapeamento de baixo custo composto por um scanner Ibeo LUX, uma antena GNSS, um Sistema de Navegação Inercial Novatel SPAN-IGM-S1, que integra um receptor GNSS e uma Unidade de Medida Inercial, um computador portátil Raspberry Pi e um octóptero. O sistema foi avaliado para o modo aéreo usando um octocóptero desenvolvido pela empresa Sensormap. A densidade de pontos resultante em área com concentração de árvores também foi avaliada. A densidade de pontos obtida com este sistema é menor que a coletada por um sistema de varredura aérea LASER convencional, mas os resultados mostram que a precisão altimétrica com este sistema é de cerca de 30 cm, que é aceitável para aplicações florestais. As maiores vantagens deste sistema são o baixo peso e baixo custo que o torna atraente para várias aplicações.

Palavras-chave: Sistema de Varredura a LASER móvel; VANT; ferramenta de mapeamento; nuvem de pontos.

1. Introduction

Unmanned Aerial Vehicles (UAVs) are becoming a cost-effective alternative to conventional aircraft for aerial image acquisition, mainly in small areas. The use of UAVs allows high frequency temporal image acquisition at lower height and speed flights, resulting in better spatial resolution and accuracy.

Small UAVs, weighting less than 20 kg, are low-cost technologies but have limited payload capacity and flight range. As they are compact platforms, the available space for the integration of equipment is limited, requiring smaller and lighter onboard systems to ensure improved autonomy.

Recent studies have used laser scanning systems onboard UAVs to characterize the three-dimensional structure of ecosystems: forestry volume, biomass estimative, carbon storage and biodiversity mapping (Jaakkola et al., 2010; Lin et al., 2011; Wallace et al., 2011; 2012 a; Wallace et al., 2012 b; 2014; Honkavaara et al., 2012; Chisholm et al., 2013; Wallace, 2013; Tulldahl and Larsson, 2014).

The main points encouraging the use of laser scanning systems for forest mapping are fast acquisition of three-dimensional data from the scene and laser penetration in vegetation, providing returns of reflected pulses from understory and terrain layers below the tree canopy in instances of aerial surveying. Laser scanning data enables the characterization of habitats and forest studies, avoiding intensive field surveys. In addition, filtering of above ground elements for digital terrain model generation is greatly facilitated. The use of laser scanner units onboard UAVs can reduce the costs and enable acquisition of data at a higher temporal rate, which could benefit several areas related to environmental monitoring and mapping.

This paper describes the development and assessment of a system for Airborne Laser Scanning (ALS) onboard small UAVs, as well as the analysis of the resulting data and assessment of pulse penetration in vegetated areas in order to validate the applicability of the system for biodiversity mapping and forestry biomass estimation.

2. Background

Mobile scanning devices require knowledge of both the position and attitude changes during the acquisition period to enable the transformation of coordinates from the device reference system to ground reference system. To achieve that, the integration of GNSS (Global Navigation Satellite System) and IMU (Inertial Measurement Unit) technologies to a mobile laser scanning system is a recommended procedure (Shan and Toth, 2008). The laser scanning unit provides mirror scan angle and distance information and the GNSS/IMU system provides the position and orientation of the sensor, but at different frequencies and time systems, making necessary the interpolation of position and attitude to the instant of laser measurement enabling the computation of point coordinates.

Ground coordinates of each point measured by the mobile laser scanner are calculated with Equation 1, adapted from Habib et al. (2010 a), which express the sum of three vectors (See Figure 1).

$$\mathrm{r}_{\mathrm{i}}^{\mathrm{g}} = \mathrm{r}_{\mathrm{GNSS}}^{\mathrm{g}}(\mathrm{t}) + \mathrm{R}_{\mathrm{IMU}}^{\mathrm{g}}(\mathrm{t})\mathrm{r}_{\mathrm{LU}}^{\mathrm{IMU}} + \mathrm{R}_{\mathrm{IMU}}^{\mathrm{g}}(\mathrm{t})\mathrm{R}_{\mathrm{LU}}^{\mathrm{IMU}}\mathrm{R}_{\mathrm{ED}}^{\mathrm{LU}}(\mathrm{t})\rho_{\mathrm{i}}(\mathrm{t}) \quad (1)$$

Where:

$\mathrm{r}_{\mathrm{i}}^{\mathrm{g}}$: Ground coordinates of point i;

$\mathrm{r}_{\mathrm{GNSS}}^{\mathrm{g}}(\mathrm{t})$: Ground coordinates of the GNSS antenna at an instant t, reduced to the IMU coordinate system;

$\mathrm{R}_{\mathrm{IMU}}^{\mathrm{g}}(\mathrm{t})$: Rotation matrix relating the ground and IMU coordinate systems at an instant t, derived after processing the GNSS and IMU data;

$\mathrm{r}_{\mathrm{LU}}^{\mathrm{IMU}}$: Offset between the laser unit and IMU origin (lever-arm);

$\mathrm{R}_{\mathrm{LU}}^{\mathrm{IMU}}$: Rotation matrix relating the laser unit and IMU coordinate systems (boresight misalignment angles);

$\mathrm{R}_{\mathrm{ED}}^{\mathrm{LU}}(\mathrm{t})$: Rotation matrix relating the laser unit coordinate system and the laser emitting devices (mirror scan angles) at an instant t. As the laser unit used in this research scans four horizontal layers, the rotation matrix is expressed as a function of two angles (β and θ).

$\rho_{\mathrm{i}}(\mathrm{t})$: Coordinates of point i expressed in the emitting device reference system.

The elements expressed in Equation 1 are measured during the acquisition process, except the lever-arm parameters which are directly measured after (or before) the mission, and the

boresight angles which are indirectly estimated in the calibration process, which can be done in laboratory or in-flight.

Habib et al. (2010 b) divide the calibration process into three steps: laboratory calibration; platform calibration and in-flight calibration. The laboratory calibration estimates the offset and orientation angles between the laser unit and the IMU coordinate systems and is generally performed by the manufacturer of commercial systems. The platform calibration establishes the offset between the laser unit and the GNSS antenna, reduced to the IMU coordinate system. The in-flight calibration uses control features to refine the estimated offset and boresight angles with in-situ data.

According to Bang et al. (2009), the calibration techniques can be classified, according to the available data, as: simplified calibration, using only the point cloud coordinates; quasi-rigorous calibration, using trajectory data and time tagged point cloud coordinates; and rigorous calibration, using raw data from the system.

The calibration process is an important step because it estimates the multiple relationship parameters among the reference systems, minimizing the discrepancies between surfaces obtained from multiple flight paths (Toth, 2002). The relationships between the coordinate systems involved in point cloud generation are shown in Figure 1.

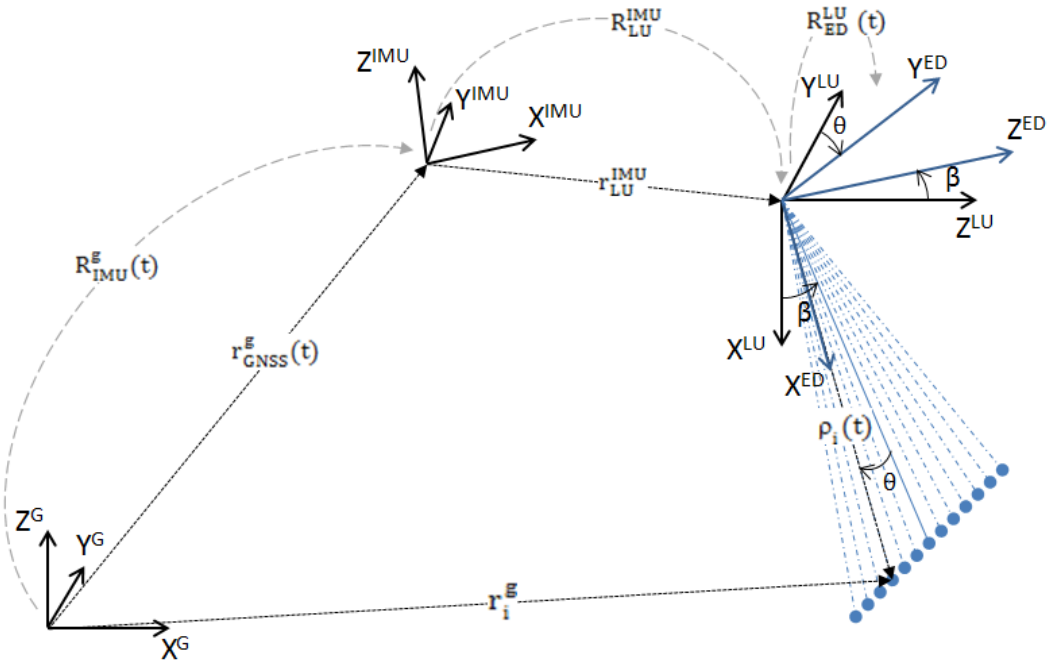

Figure 1: Relation between the coordinate systems involved.

The calibration processes are also based on Equation 1 which is manipulated to compute the boresight angles as a function of known data (see section 4 and Tommaselli and Torres, 2016). When raw data is available, the *boresight* angles can be left as unknowns and solved based on control points coordinates, control features or common features between strips (Burman, 2000; Toth, 2002; Skaloud and Lichti, 2006; Habib et al., 2010 b).

Experimental systems have the advantage of gathering access to all raw data, allowing rigorous calibration, which is not common with commercial integrated systems, that provides only the final results. Some research projects are developing experimental light-weight laser scanning systems to be carried by UAVs for mapping purposes. Jaakkola et al. (2010) presented the Sensei system: a light-weight system based on an Ibeo Lux laser scanner, a Sick LMS laser profiler, a SPAN-CPT INS (Inertial Navigation System), a spectrometer and a CCD camera, carried by a helicopter UAV. This system was tested for tree measurements and for pole detection, road extraction, and digital terrain model refinement (Lin et al., 2011).

Wallace et al. (2012 a) developed a similar system, but integrating an Ibeo Lux laser scanner, a low-cost IMU and a video-camera, from which exterior orientation parameters were estimated, carried by an octopter UAV for forestry inventory purposes.

Glennie et al. (2013) integrated a Velodyne HDL-32E laser scanner to an OxTS IMU and performed experiments in terrestrial mode and with the system carried by a balloon at 25 m and 30 m of flight height, achieving an altimetric accuracy at centimeter level.

Adler et al. (2014) presented an octopter UAV with an INS and a Hokuyo UTM-30LX laser range finder integrated for autonomous exploration of urban environments. The results achieved showed that the system can be applied for motion planning and collision avoidance, and in applications of surface reconstruction.

The system described in this paper has similar components to those cited above. The payload weighs about 3 kg, the UAV has more autonomy to perform longer flights and the INS has not been used in other systems. The system components will be detailed in the next section. The experiments were also performed at greater flight heights compared to previous papers.

3. System description

The UAV system used in this study is composed of an Inertial Navigation System (INS) (Figure 2-a) integrating GNSS/IMU solutions to provide position and orientation of the platform, a laser scanner unit (Figure 2-b) and a Raspberry PI portable computer (Figure 2-c) that controls data acquisition and records raw laser data and binary data from the INS for later post-processing.

The positioning and orientation system is a Novatel SPAN-IGM-S1, composed by a dual frequency GNSS OEM615 receiver and a Sensonor's STIM300 MEMS IMU, which integrates the raw inertial measurements with all available GNSS information to provide a better solution to the IMU measurements' systematic errors or GNSS signal loss. The IMU data is usually grabbed with 125 Hz frequency and the GNSS data with 10 Hz. The GNSS receiver is also responsible for the time synchronization of the laser scanner via Pulse per Second (PPS) signal and National Marine Electronics Association (NMEA) messages sent to the laser unit, which provides synchronization with errors around 1 ms, which is suitable considering the UAV flight speed. Data processing is usually done by relative positioning in kinematic mode, using a GNSS base station. In this project the GNSS and IMU data were processed with the Inertial Explorer software, from Novatel.

The laser scanner unit is an Ibeo LUX 2010 from Ibeo Automotive Systems GmbH which was developed to drive assistance. The Ibeo LUX scans four parallel levels with different vertical angles (3.2° of amplitude between the lower and the higher levels) and records up to three

echoes per laser pulse transmitted. It can also be configured to scan at three different frequencies (12.5 Hz, 25 Hz and 50 Hz) and with a limited angular aperture (up to 110° for the horizontal angular scan). For the experiments described in this paper, the laser unit was configured to operate at a scan frequency of 25 Hz, which results in a pulse repetition frequency of around 20 kHz, and with an angular aperture of 60° (+ 30° to – 30°). Scan angle values and measured distances are provided by this scanner but it does not grab the intensity information of the reflected pulse, only its width. The nominal accuracy of the measured distance is 10 cm.

Studies applying an Ibeo LUX unit onboard UAV for forestry inventory, identification of individual trees and biomass estimative are shown in Jaakkola et al. (2010), Wallace et al. (2011; 2012 a), Wallace et al. (2012 b; 2014) and Lin et al. (2011). In Wallace et al. (2012 a) high definition video data was used to improve the solution achieved by a lower grade GNSS/IMU positioning and orientation system.

Weight and size are important features bearing in mind the UAV's payload restrictions. The UAV platform used in the aerial experiments described in this paper is a UAV octopter (Figure 2-d) developed by a third partner company (Sensormap Geotecnologia). It weighs about 13 kg and it is able to carry a payload of 5 kg for a 30 min mission.

The UAV performs flights controlled by a radio system. Initial terrestrial experiments were performed with the system components fixed on the roof of a terrestrial vehicle (Figure 2-e). For both experiments, terrestrial and aerial, the laser unit and the INS were installed on a rigid support to mitigate against vibration and offsets between them during data acquisition.

The physical integration system, with a communication and power distribution box connecting the sensors, was also developed by a third part company.

As the integrated sensors work at different frequencies and time systems, it is important that the measurements of all sensors be referenced to the same time system. To achieve this, the position and attitude measurements are interpolated to the same instant of the laser measurements, with linear interpolation.

The sensors were synchronized to GPS time because of its stability and precision. The developed communication box is also responsible for the PPS signal conversion, provided by the GNSS antenna at TTL (Transistor-to-Transistor Logic) level, into RS232 (Recommended Standard 232) level, so that it is recognized and synchronized by the laser unit system.

In addition to time synchronization, it is important to verify the mounting orientation of the sensors to know the relation between their coordinate systems for the point cloud calculation. The interpolation of GNSS/INS measurements and point cloud calculation are performed by an in-house implemented C++ program using linear interpolation, which is suitable to this type of trajectory and data. Some restrictions to the inputted laser data were also implemented on the C++ program to eliminate spurious data.

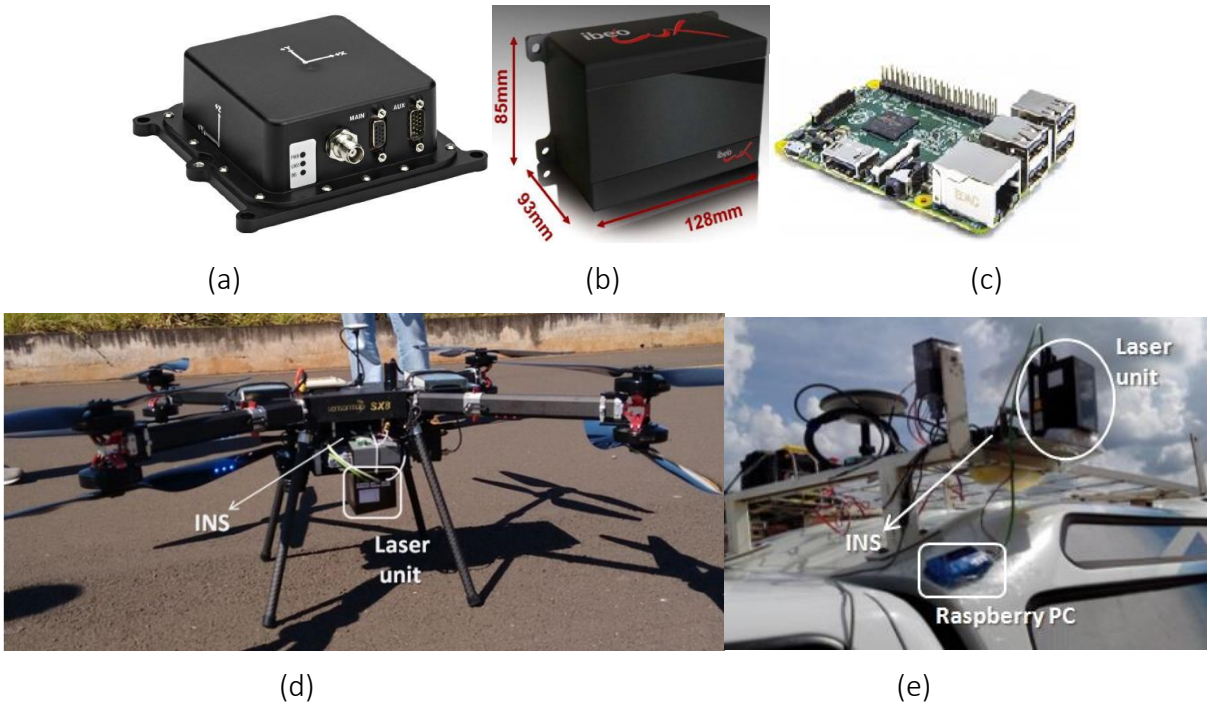

Figure 2: Main components of the light-weight laser scanner system (a) INS; (b) laser scanner; (c) Raspberry PI; (d) UAV octopter; (e) system installed on mobile terrestrial vehicle.

4. Calibration and quality control

Calibration and quality control were based on Ground Control Points extracted from natural features, existing at the scenes, and artificial targets. Their location in the cloud points was performed manually. Kager (2004), Wotruba et al. (2005), and Csanyi and Toth (2007) described methods for quality control of laser point clouds using specially designed targets for absolute control and different flight strips for relative control.

Only altimetric quality control was performed in areas with no identifiable points in the point cloud, using a reference point cloud, if available, or GCPs distributed at the scene and obtained by GNSS surveying.

Raw measurements were then used to calculate laser unit position, attitude, scan angles and distance which were extracted and applied in Equation 2. Assuming the element r_i^g as the coordinates of GCPs obtained by GNSS surveying and leaving the *boresight* angles as unknowns leads to Equation 2.

$$R_{IMU}^{g}(t)^{-1} * \left[r_i^g - r_{LS}^g(t)\right] = R_B R_{LU}^{IMU} r_i^{UL}(t) \quad (2)$$

Where:

$r_{LS}^g(t) = r_{GNSS}^g(t) + R_{IMU}^g(t) r_{LU}^{IMU}$, is the laser unit position in the geodetic reference system;

$r_i^{LU}(t) = R_{ED}^{LU}(t) r_i^{ED}$, is the point position in the laser unit reference system;

R_{LU}^{IMU} is the rotation matrix that relates the laser unit and IMU coordinate systems as a function of the approximate angles directly measured ($\Delta\kappa, \Delta\varphi, \Delta\omega$); and

R_B is the rotation matrix related to the misalignment correction in function of the unknown angles (dω, dϕ, dκ), given by $R_Z(d\kappa)R_Y(d\varphi)R_X(d\omega)$ multiplication.

For the onboard UAV case, as the mounting arrangement of the systems is always the same, the R_{LU}^{IMU} elements are given as: $\Delta\kappa$ = -90º, $\Delta\varphi$ = -90º and $\Delta\omega$ = 0º.

The elements of the R_B matrix can be estimated and adjusted by the parametric method (Gauss Markov) and, then, a new point cloud processing is executed with the correction of the *boresight* angles estimated.

Quality control was based on coordinate discrepancies of identifiable points and/or altimetric differences between point clouds.

5. Experiments and results

A preliminary test was performed with a mobile terrestrial platform to analyze data consistency with ground truth. The facade of a building (Figure 3-a) was scanned in a single path and then the resulting point cloud (Figure 3-b) was compared to a dense reference point cloud obtained by an MDL DynaScan M150 laser scanner, with an accuracy of 5 cm, also in terrestrial mode. The continuous line shown in Figure 3-b represents the vehicle's trajectory and the calculated point cloud is colored in function of elevation. Some gaps in the point cloud that were caused by corrupted data packages were eliminated in the filtering steps. These gaps can be seen in Fig. 3-b and 3-c. The filtering process was executed by an in-house implemented C++ program with the aim of validating the laser data and removing noisy observations. The filtering process implemented in C++ analyses the coherence of the data extracted from the binary file, for instance, the layer numbers, the angles codes, the distances values and pulse width, from previously defined thresholds.

Both point clouds were superimposed aiming the comparison and are presented in Figures 3-c and 3-d. The superimposition of the point clouds was made using a point cloud visualization software (FugroViewer). Both point clouds were generated in the same coordinate reference system (WGS84), so the superimposition was directly achieved by merging the point clouds. Figure 3-c shows an oblique view of both point clouds and Figure 3-d is a top view from which the offset between the point clouds in relation to the lateral wall of the building can be seen. This offset is around 0.8 meters and can be explained by a combined effect of attitude errors and footprint divergence. Attitude errors can have a systematic component caused by the boresight misalignment angles, which were not corrected in this experiment. The footprint is elongated in the horizontal direction, making objects to appear wider in the trajectory direction, considering that the laser unit was mounted vertically with respect to the observed object. Errors in attitude angles can be explained both by the lack of correction of the boresight misalignment errors and by the low velocity of the platform, causing large accumulation of errors in the accelerometers and gyroscopes. The distance measurement nominal accuracy also has an influence on the offset. It is important to emphasize that this experiment was a proof of concept and that the errors were reduced in the aerial case.

The reference point cloud was filtered to represent only the walls of the building and the calculated point cloud presents points of ground and points resulting from pulse returns of objects inside the building, since laser pulses passed through the glass of windows in the facade.

(a)

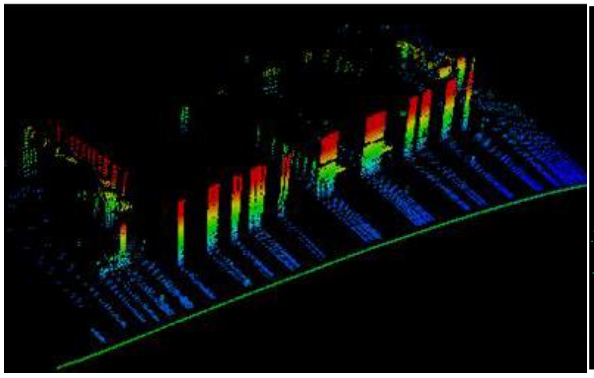

(b)

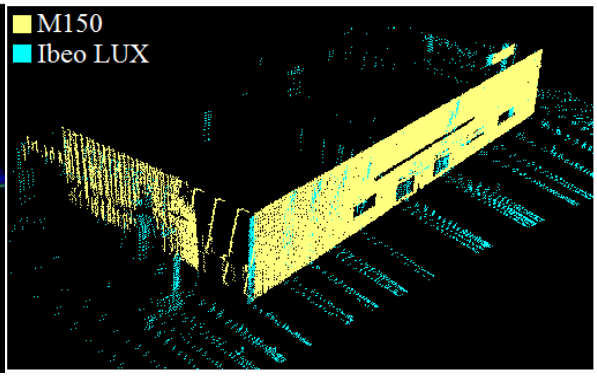

(c)

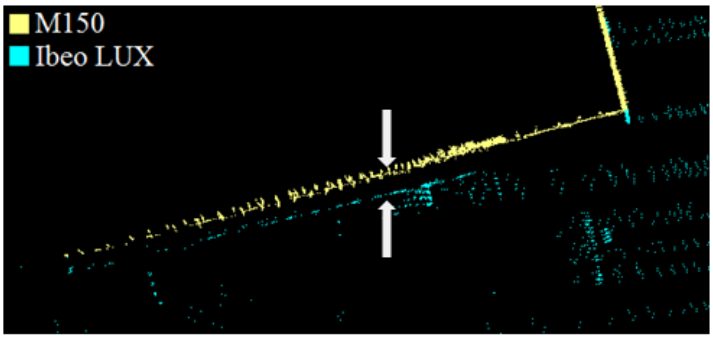

(d)

Figure 3: (a) The facade of the building scanned; (b) calculated point cloud; (c) superimposition of the reference point cloud and the calculated point cloud for comparison; (d) detail of the offset between the point clouds.

After the terrestrial tests in which system point cloud characteristics were assessed, some tests were performed with the system carried by the UAV.

The first experiment was made over a parking area (Figure 4-a) with a flight height of 100 m. The standard deviations obtained from the GNSS and IMU data processed with Inertial Explorer were 0.013 m and 0.014 m for planimetric and altimetric coordinates, respectively, 0.0059° for ω and ϕ components and 0.060° for κ. The resulting point cloud is presented in Figure 4-b. The digital terrain model generated by this point cloud, with 1 meter spacing, is shown in Figure 4-c.

The black central area in Figure 4-b corresponds to points with no pulse returns due to the low reflectivity of the black pavement for the flight height of 100 m. However, a small area with dense pulse returns from the black pavement can be seen in Figure 4-b-2 (in cyan). Those pulses were received when the UAV was landing and the flight height was decreasing (about 60 m above ground). From these results it can be concluded that 60 m was a favorable flight height from which to get a dense sampling even for low reflectivity targets.

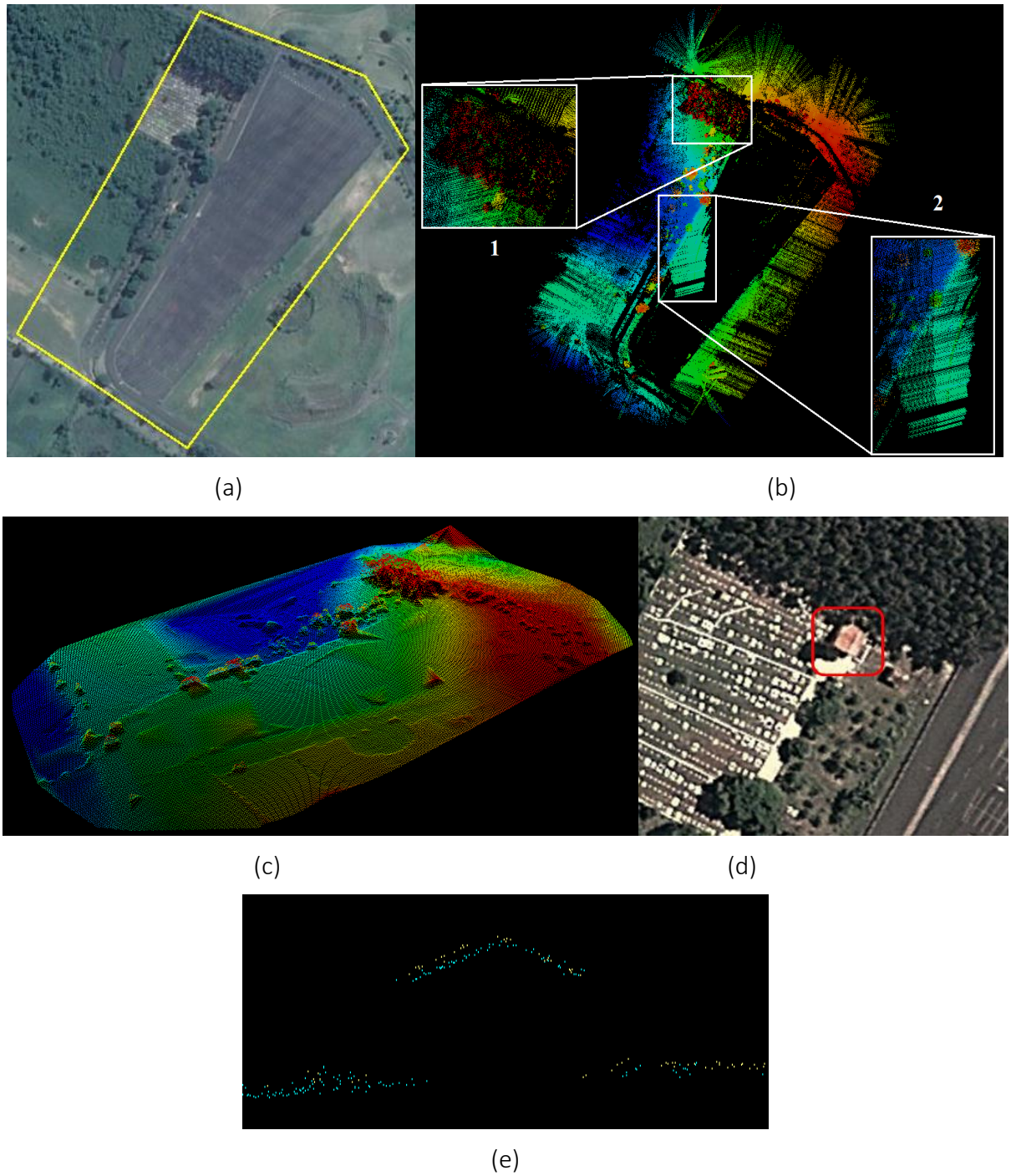

Figure 4: First experiment: (a) Area covered; (b) calculated point cloud; (c) DSM from the resulting point cloud; (d) building used for relative quality control and (e) profile of a point cloud sample obtained from two flight lines.

The pulse penetration in the tree canopy was analyzed in a region of dense vegetation (see Figure 4-b-1). Three 5x5 m samples were analyzed for the point density estimative. The mean point density for each sample was 45 points (1.8 points/m²), from which 19 were from the ground. This analysis shows that it would be feasible to estimate average tree heights from this data and to generate canopy height models (CHM).

As the identification of control points for the quality control and calibration process in this area is difficult, only the altimetry quality analysis was performed. The ground coordinates of nine points distributed in the parking area were obtained by GNSS surveying and their elevations were compared to the values interpolated from the point cloud. The discrepancies presented an average value of 0.11 m and the standard deviation of 0.18 m, and an RMSE of 0.20 m.

A relative quality control was also performed using the estimated rooftop corners of a building (Figure 4-d and e) existing in the area. The building rooftop was observed from two flight lines and Figure 4-e shows the profile of the resulting point cloud in that area. The discrepancy in the elevations of the rooftop corners measured in point clouds from two flight strips was 0.21 m.

Altimetric errors are affected by planimetric errors and this relationship is dependent on the terrain slope and altitude variations. In the study area the altitude varies 4 meters from north to south limits of the area.

The second study area was an urban park with dense vegetation (Figure 5-a). The experiments were performed to analyze pulse penetration and accuracy in flat areas. To facilitate ground control identification and location points, special targets were distributed over the area. Two flight heights were used in this experiment, 60 m and 75 m, in order to analyze the influence of flight height on pulse returns and point density.

Nine flight lines were performed. The resulting point clouds were divided into two blocks, according to the direction of the flight lines. Figure 5-b shows the complete point cloud generated and Figure 5-c presents an East-West point cloud profile containing an isolated building and trees. The flight line directions are shown in Figure 5-d.

For the calibration process and quality analysis, artificial flat targets of 90 x 90 cm square panels to be installed over tripods were designed (Figure 5-e). The targets were distributed over flat areas in such a way as to be identified in point clouds based on slope change (Figure 5-e). Natural features in the scene were also used to enable both *boresight* estimation and accuracy assessment, as two cars and a building present on the scene.

Due to low point density and gaps in data recording, from the 7 GCPs installed only 4 could be identified in point cloud. The coordinates of all targets were obtained by GNSS positioning and compared to the estimated targets positions in point cloud for absolute quality control. The average values, standard deviation and RMSE are shown in Table 1.

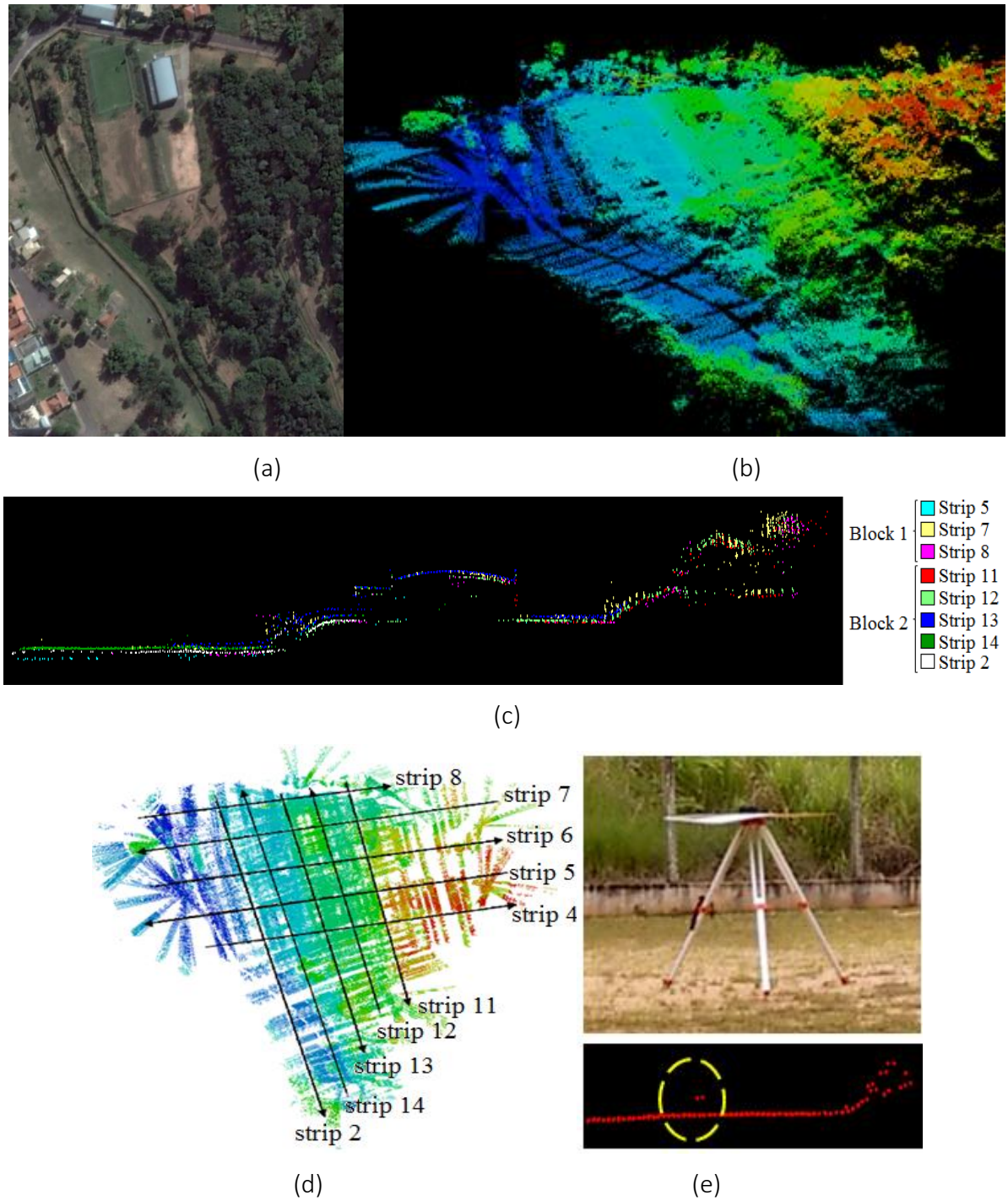

Figure 5: (a) Second study area; (b) resulting point cloud; (c) lateral profile sample containing an isolated building (center) and trees (right); (d) localization of flight lines; (e) target example and its identification in point cloud.

For this second flight, the standard deviations obtained from the GNSS and IMU data processed with Inertial Explorer were 0.13 m and 0.17 m for planimetric and altimetric coordinates, respectively, 0.0089° for ω and ϕ components and 0.1101° for κ.

The calibration process was implemented and the *boresight* parameters were estimated using 3 strips that have 4 GCPs identifiable. The estimated values of the boresight angles are:

d□ = 0.222°, d□ = 0.085° and d□ = -1.406°. The standard deviation of the estimated boresight angles were: □□ = 0.386°, □□ = 0.322° and □□ = 1.383°. Even considering the high standard deviation in the angles, compared to the estimated values, the obtained results, using the estimated *values*, improved slightly over the point cloud computed with the initial values for *boresight* misalignment (see Table 1, columns (b)).

Table 1: Errors for GCPs measured in point clouds with 3 strips (2, 12 and 13) (a) before and (b) after the calibration procedure, and (c) with strip 12 removed from the data.

	(a)			(b)			(c)		
	ΔX (m)	ΔY (m)	ΔZ (m)	ΔX (m)	ΔY (m)	ΔZ (m)	ΔX (m)	ΔY (m)	ΔZ (m)
Mean	-0.047	0.632	-0.32	-0.169	0.398	-0.304	-0.285	0.192	0.075
Standard Deviation	0.488	0.814	0.501	0.418	0.322	0.509	0.465	0.264	0.251
RMSE	0.454	0.983	0.564	0.422	0.497	0.560	0.493	0.299	0.230

According to Jaakkola et al. (2010) and Wallace et al. (2012 a), the noise caused by the resolution and accuracy of the laser scanner and laser spot size, which is wider in the horizontal direction, is larger than the misalignment errors and, as a consequence, in some cases the *boresight* angles can be considered negligible. In this set of experiments, it can be seen that the accuracy in Y was better after using the estimated *boresight*, while X and Z improved marginally.

Further analysis was performed to explain the values of the discrepancies, which were not compatible with the first experiments. The three strips in which GCPs appeared were assessed and strip 12 showed systematic effects in the Y and Z coordinates of around 1.20 m and 0.80 m, respectively. These errors were probably caused by non-modeled systematic errors in the platform position and attitude which could not be detected. The measurements in the GCPs from this strip were eliminated and the RMSE reduced to 0.23 m in height (see Table 1, columns (c). The RMSEs for these strips were within the expected accuracy for this system. It is important to mention that the values for planimetric errors are largely affected by uncertainty when locating the GCP in the cloud points, due to the low spatial frequency of this device (see Figure 5-e).

Another quality analysis was performed using a reference point cloud obtained by an aerial survey using a RIEGL LMS Q680i laser scanner performed by the Engemap company. The reference point cloud was resampled to a grid with 1 m spacing, as shown in Figure 6-a. The altimetry accuracy of this reference point cloud is around 15 cm.

The point clouds of two blocks (see Figure 6-b and 6-c) were compared to the reference data. The first block presented around 11% of discrepancies below 0.25 m, and the second block presented around 19 %. High discrepancies were mostly in vegetated areas and in the isolated edification edges. These high discrepancies can be explained by horizontal errors that contribute to the estimated altimetric error. The horizontal errors are caused by a combined effect of position and attitude errors in the platform (computed from GNSS and IMU data), non-modeled *boresight* misalignment and laser footprint. The discrepancies between the generated point clouds and the reference data are shown in Figure 6-d (Block 1) and 6-e (Block 2). The effects of

the elongated laser footprint in the flight direction can be seen in the discrepancies around areas with high gradients, for instance, the building.

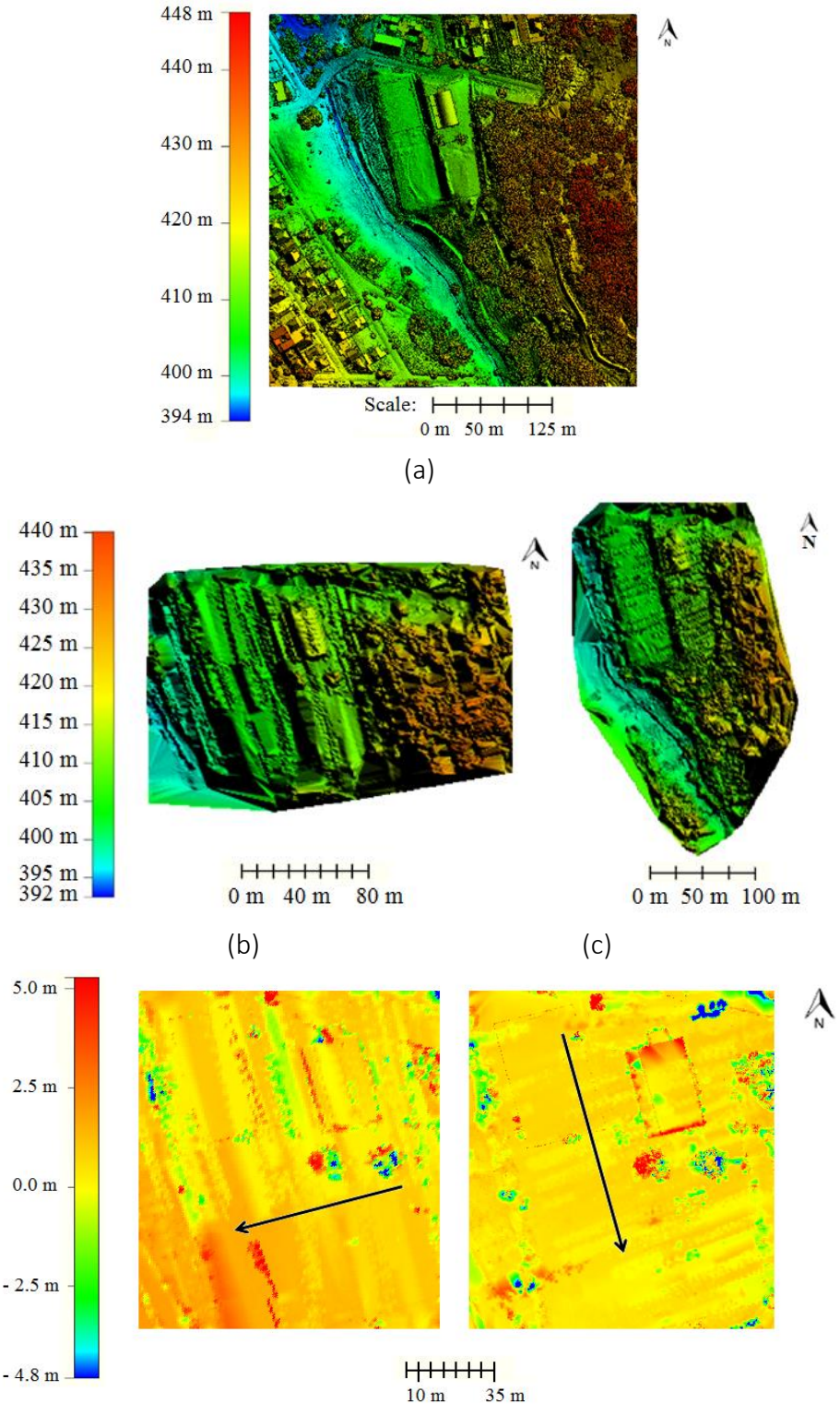

Figure 6: DSM coloured by the altitude: (a) Reference DSM with 1m GSD; (b) and (c) DSM with 1m GSD obtained from block 1 and block 2 point clouds; colored by discrepancies in altitude: (d) and (e) grids with discrepancies obtained from two blocks compared to the reference DSM with the flight directions for each block indicated.

The pulse penetration analysis in the dense vegetation area was also based on 3 samples with 5x5 m. The average point density for each sample was 129 points (5 points/m²), from which 11 reached the ground. This analysis showed a good point density when compared to the experiment at 100 m flight height, with the potential to estimate the average height of trees in a more vegetated area.

5. Conclusion

This paper presents the development and assessment of a light-weight laser scanner system onboard an UAV, with experiments under different configurations to estimate its accuracy and point density. The features of this system related to weight and cost are quite attractive for several applications. This system can be improved with the integration of other sensors, such as an RGB digital camera and a second dual frequency receiver to improve heading estimation.

Summarizing the advantages of this system in comparison with the existing systems (Jaakkola et al. (2010) and Wallace et al. (2012 a)), this prototype integrated a different INS (lower cost), and it is able to perform longer flights within heavier payloads, allowing its use with high flexibility. The experiments were performed in different conditions, mainly at a flight height of 100 m (higher). Experiments with system calibration were also presented. One important contribution of this work was the development of the software for cloud point generation from the raw measurements coming from the laser unit and from the INS. Even with a lower point density, the presented results are consistent with those achieved by other authors using similar laser systems. Altimetric accuracy with this prototype is better than 30 cm, which is acceptable for forest applications.

In future research, a second GNSS receiver will be integrated to improve heading computation. Also, the feedback event of every mirror cycle will be marked in the GNSS receiver, enabling future analysis of the angular errors due to mirror speed variations. The causes of data loss generating gaps in the point clouds will be also assessed in future work.

ACKNOWLEDGEMENTS

The authors would like to acknowledge the financial support from FAPESP (Fundação de Amparo à Pesquisa do Estado de São Paulo - grant 2013/50426-4) and CAPES (Coordenação de Aperfeiçoamento Pessoal de Nível Superior - grant 307554/2014-7), and the data provided from the third partner company, Sensormap Geotecnologia. The technical and scientific support given by the Finish Geospatial Institute (FGI), with the researchers Eija Honkavaara and Anttoni Jaakkola are also greatly acknowledged

REFERENCES

Adler, B.; Xiao, J. and Zhang, J. 2014. Autonomous Exploration of Urban Environments Using Unmanned Aerial Vehicles. *Journal of Field Robotics*, 31(6), pp. 912–939. doi: 10.1002/rob.21526

Bang, K. I.; Habib, A. F. and Müller, M. 2009. Lidar System Calibration Using Overlapping Strips. *Boletim de Ciências Geodésicas*, 15(5), pp. 725-742.

Burman, H. 2000. *Calibration and Orientation of Airborne Image and Laser Scanner Data Using GPS and INS*. PhD. Royal Institute of Technology.

Chisholm, R. A.; Cui, J.; Lum, S. K. Y. and Chen, B. M. 2013. UAV LiDAR for below-Canopy Forest Surveys. *Journal of Unmanned Vehicle Systems*, 1(1), pp. 61–68.
doi: 10.1139/juvs-2013-0017.

Csanyi, N. and Toth, C.K. 2007. Improvement of lidar data accuracy using lidar-specific ground targets. *Photogrammetric Engineering & Remote Sensing*, 73(4), pp. 385–396.
doi: 10.14358/PERS.73.4.385.

Glennie, C.; Brooks, B.; Ericksen, T.; Hauser, D.; Hudnut, K.; Foster, J. and Avery, J. 2013. Compact Multipurpose Mobile Laser Scanning System - Initial Tests and Results. *Remote Sensing*, 5(2), pp. doi: 521-538. 10.3390/rs5020521.

Habib, A.; Kersting, A.P.; Bang, K.I.; Lee, D.C. 2010a. Alternative Methodologies for the Internal Quality Control of Parallel LiDAR Strips. *IEEE Transactions on Geoscience and Remote Sensing*, 48(1), pp. 221–236. doi: 10.1109/TGRS.2009.2026424.

Habib, A.; Bang, K.I.; Kersting, A.P. and Chow, J. 2010b. Alternative Methodologies for LiDAR System Calibration. *Remote Sensing*, 2(3), pp. 874-907. doi: 10.3390/rs2030874.

Honkavaara, E.; Kaivosoja, J.; Mäkynen, J.; Pellikka, I.; Pesonen, L.; Saari, H.; Salo, H.; Hakala, T.; Marklelin, L.; Rosnell, T. 2012. Hyperspectral reflectance signatures and point clouds for precision agriculture by light weight UAV imaging system. *ISPRS Annals Photogrammetry, Remote Sensing and Spatial Information Sciences*, I-7, pp. 353–358.

Jaakkola, A.; Hyyppä, J.; Kukko, A.; Yu, X.; Kaartinen, H.; Lehtomäki, M. and Lin, Y. 2010. A low-cost multi-sensoral mobile mapping system and its feasibility for tree measurements. *ISPRS Journal of Photogrammetry and Remote Sensing*, 65(6), pp. 514–522.
doi: 10.1016/j.isprsjprs.2010.08.002.

Kager, H. 2004. Discrepancies between overlapping laser scanner strips–simultaneous fitting of aerial laser scanner strips. *International Archives of Photogrammetry, Remote Sensing and Spatial Information Sciences*, 35(B1), pp. 555–560.

Lin, Y.; Hyyppä, J. and Jaakkola, A. 2011. Mini-UAV-borne LIDAR for fine-scale mapping. *Geoscience and Remote Sensing Letters, IEEE*, 8(3), pp. 426–430.
doi: 10.1109/LGRS.2010.2079913.

Shan, J. and Toth, C. K. 2008. *Topographic Laser Ranging and Scanning*: Principles and Processing. Taylor & Francis. doi: 10.1201/9781420051438.

Skaloud, J. and Lichti, D. 2006. Rigorous approach to bore-sight self-calibration in airborne laser scanning. *ISPRS Journal of Photogrammetry and Remote Sensing*, 61(1), pp. 47–59. doi: 10.1016/j.isprsjprs.2006.07.003.

Tommaselli, A. M. G. and Torres, F. M. 2016. A light-weight laser scanner for UAV applications. *International Archives of the Photogrammetry, Remote Sensing & Spatial Information Sciences*, 41(B1), pp. 12-19.

Toth, C. K. 2002. Calibrating airborne lidar systems. *Proceedings ISPRS Commission II Symposium*, pp. 475–480.

Tulldahl, H. M. and Larsson, H. 2014. Lidar on small UAV for 3D mapping. *Proceedings of the SPIE*, 925009.

Wallace, L.; Lucieer, A.; Turner, D. and Watson, C. 2011. Error assessment and mitigation for hyper-temporal UAV-borne LiDAR surveys of forest inventory. *Proceedings of Silvilaser*, pp. 1-13.

Wallace, L.; Lucieer, A.; Watson, C. and Turner, D. 2012a. Development of a UAV-LiDAR System with Application to Forest Inventory. *Remote Sensing*, 4(6), pp. 1519-1543. doi: 10.3390/rs4061519.

Wallace, L.; Lucieer, A. and Watson, C. 2012b. Assessing the feasibility of UAV-based LiDAR for high resolution forest change detection. *12th Congress of the International Society for Photogrammetry and Remote Sensing*, 39(B7), pp. 499–504. doi: 10.5194/isprsarchives-XXXIX-B7-499-2012.

Wallace, L. 2013. Assessing the stability of canopy maps produced from UAV-LiDAR data. *2013 IEEE International Geoscience and Remote Sensing Symposium - IGARSS*, pp. 3879–3882. doi: 10.1109/IGARSS.2013.6723679.

Wallace, L.; Lucieer, A. and Watson, C.S. 2014. Evaluating tree detection and segmentation routines on very high resolution UAV LiDAR data. *Geoscience and Remote Sensing, IEEE Transactions*, 52(12), pp. 7619–7628.

Wotruba, L.; Morsdorf, F.; Meier, E.and Nüesch, D. 2005. Assessment of sensor characteristics of an airborne laser scanner using geometric reference targets. *International Archives of Photogrammetry and Remote Sensing*, 36(3/W19), pp. 1–6.